Master of Science Thesis
VT2019

Optimization of Simultaneous Multi Slice EPI for clinical fMRI

Andrea Fingerhut

Supervisors

Peter Mannfolk

Department of Medical Radiation Physics,
Faculty of Science
Lund University
www.msf.lu.se

Abstract

Functional MRI is a method used to map brain functionality, where the blood oxygen level (BOLD) imaging method is frequently used. Stimulation of neurons leads to an increase in energy and oxygen consumption and signal can be detected since oxygen changes the magnetic properties of the blood. In order to measure the signal variation, a fast pulse sequence is required. The purpose of this master thesis was to examine multiband EPI, which compared to the standard EPI, excite several slices simultaneously. Even though this technique leads to an improvement in the temporal resolution, it also gives a decrease in the temporal signal to noise ratio and more pronounced artifacts which increases with the acceleration factor. Hence, it can be assumed that an optimal acceleration factor exists, where temporal resolution gains and decreased temporal resolution are balanced out. Phantom measurements were first performed using three head coils (20, 32 and 64 channels). From the phantom measurements a volunteer protocol was set up. Based on ten volunteers, the area of activation and activation strength were determined. A comparison with the standard technique was made for the 20 and 64 channel coils. Based on the volunteer results, a complementary study with an incomplete paradigm was set up in order to examine the gain when using multiband clinically if the patients are non-compliant. An increase in BOLD-sensitivity was seen in moderately accelerated images when using the 64 channel head coil, which can be beneficial to use in a clinical setting. No advantage with multiband EPI could be seen when using the 20 channel head coil. Because only one volunteer was examined, no conclusions could be drawn from the study with an incomplete paradigm. However, the results indicate that it can be beneficial with multiband in a clinical case of a non-compliant patient.

Utvärdering av snabbare bildtagningsteknik i funktionell MR

I funktionell MR (fMRI) studeras aktivering i hjärnan som respons på stimuli. Detta stimuli kan bestå av flera olika uppgifter som patienten gör under bildtagningen, där uppgifterna är beroende av vilken funktion eller del av hjärnan som ska undersökas. Funktionell MR är en teknik som till exempel kan användas innan en operation av hjärnan för att i största mån undvika att skada funktionellt viktiga delar. Funktionell MR används också frekvent i forskningssammanhang. Vid ett stimuli kommer hjärncellerna i området kopplat till den specifika övningen att kräva mer energi och syre. Därför kommer både blodflödet till området och mängden syre i blodet att öka. Syre ändrar de magnetiska egenskaperna hos blodet och kommer på så sätt ge en signalökning. Uppgiften görs flera gånger med vila emellan i ett så kallat paradigm. En signal som går upp och ner kommer därför att erhållas. Denna signal jämförs mot en modell som beskriver hur förloppet borde se ut. Detta görs för att kunna avgöra om en aktivering i området har skett. Om överenstämmelsen med modellen är tillräckligt bra räknas det som en aktivering. En typisk funktionell MR-bild kan ses nedan där de röda områdena är de aktiverade områdena .

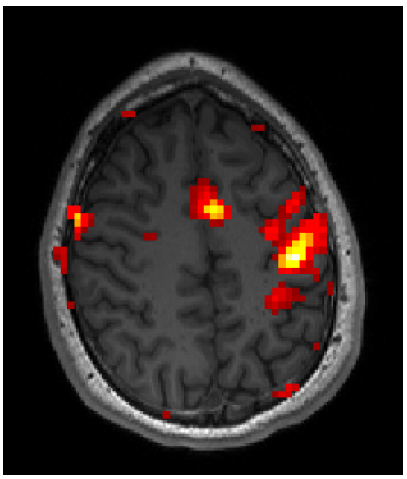

Exempel på en typisk fMRI-bild

För att kunna mäta denna signalvariation behövs en snabb bildtagningsteknik. I den teknik som används idag avbildas ett snitt i hjärnan i taget. Syftet med detta arbete är att utvärdera och optimera en teknik som gör det möjligt att bildge flera snitt i taget, kallat att accelerera bildtagningen. Det gör att själva bildtagningen kan gå snabbare. Olika accelerationer kan användas, där en acceleration på två innebär att två snitt i taget avbildas. Det gör det möjligt att antingen minska bildtagningstiden eller ta fler bilder men under samma tid som för standardmetoden. Fler bilder innebär att man kan se förändringarna hos signalen bättre, men det innebär även en försämrad bildkvalité. Uppgiften är därför att hitta den optimala accelerationen för att kunna se så små förändringar hos signalen som möjligt utan att bildkvalitén blir för dålig.

Tekniken att bildge flera snitt samtidigt kommer att undersökas för att kunna implementeras i kliniken och har därför gjorts på friska volontärer. Volontärerna fick i uppgift att utföra en övning där tummen trycktes lätt mot var och en av de andra fingrarna i följd för att få aktivering i området som har att göra med motorik. Bilderna utvärderades sedan genom att områdena som var aktiverade jämfördes med standardbildtagningen där bland annat storleken på det aktiverade området mättes samt hur stark aktiveringen var. När en MR-undersökning görs fångas signalen upp genom att en spole som mäter signal placeras runt om området som ska undersökas. Spolen kan bestå av olika antal element som fångar upp signalen. Spolar med olika antal element användes i studien och beroende på vilken spole som användes erhölls olika resultat. Det visade sig vara en fördel att accelerera bildtagningen med två när en spole med många element användes för att fånga upp signalen. Det innebar att dubbelt så många bilder kunde tas jämfört med standardbildtagningen. Dock var det

ingen direkt skillnad mellan bildtagningsteknikerna då färre element användes.

List of abbreviations

ACS - Auto calibration signal

BOLD - Blood oxygen level dependent

CAIPIRINHA - Controlled aliasing in parallel imaging results in higher acceleration

EPI - Echo planar imaging

FA - Flip angle

fMRI - Functional magnetic resonance imaging

FOV - Field of view

FWHM - Full width half maximum

GLM - General linear model

GRAPPA - Generalized autocalibrating partial parallel acquisition

GRE - Gradient echo

HRF - Haemodynamic response function

MEG - Magnetoencephalography

MPRAGE - Magnetization prepared rapid gradient echo

PET - Positron emission therapy

PINS - Power independent number of slices

RF - Radiofrequency

SAR - Specific absorption rate

SENSE - Sensitivity encoding

SMS - Simultaneous multi-slice

TE - Echo time

TR - Repetition rime

tSNR - Temporal signal to noise ratio

Contents

1 INTRODUCTION

Preoperative evaluation of brain functionality is important in order to perform safe neurosurgery. The functionality is unique for every brain and diseases can change the functional anatomy. The brain mapping can therefore not be generalised and individual assessments have to be made before each surgery. There are several noninvasive methods that can be used to evaluate functionality such as positron emission tomography (PET), magnetoencephalography (MEG), and functional magnetic resonance imaging (fMRI) [1]. Functional magnetic resonance imaging is one of the dominating methods in both clinical and cognitive neuroscience and is a method where activation in different parts of the brain is studied during stimuli using magnetic resonance. It has the advantage of being easily accessible as most hospitals already have a high field MRI-scanner. It is also capable of mapping the whole brain and uses non ionising radiation [1].

Early studies using PET show that the cerebral blood flow overshoot the oxygen metabolism [2]. This gives a net increase in the ratio between the oxygenated capillary arterial blood and the deoxygenated venous blood which can be measured [3]. This is called blood oxygen level dependent contrast fMRI (BOLD-fMRI). To image these changes, fast pulse sequences are needed and therefore 2D GRE-EPI is traditionally used. There have been several developments in order to shorten the acquisition time where parallel imaging, which only samples parts of the k-space, is widely used. This is called in-plane acceleration and has been made possible because of innovative reconstruction methods such as SENSE and GRAPPA [4]. One technique to reduce image acquisition time even more is to excite several slices simultaneously, called slice acceleration. This technique is named multiband or simultaneous multislice and has been made possible by the development of CAIPIRHINIA which shifts the slices relative to each other [5]. Different number of simultaneous excited slices can be used which gives different acceleration factors. A higher acceleration factor decreases the shortest available repetition time (TR) of the imaging sequence.

1.1 Aim

Guiding the planning of epilepsy and tumour surgery is the most common application of clinical fMRI [1]. For this, a good temporal resolution is required. Multiband EPI can be used to improve the temporal resolution by sampling more data during the same time as traditional EPI, but even though this leads to an increase in the temporal resolution, it also gives a reduction in image quality. Multiband EPI induces a higher noise level, which originates from the aliased signals and image artefacts such as signal leakage between simultaneous excited slices [6]. The aim of this project is to find an optimal acceleration factor to achieve as good temporal resolution as possible without compromising the data quality. Previous studies have examined this pulse sequence, but during this master thesis an investigation of how the pulse sequence can be implemented in a clinic setting will also be made [5, 6]. This implies studying relevant combinations of coils and acceleration factors, in order to determine an optimal clinical setting. Patients can have difficulties performing tasks while in the MRI-scanner. Therefore a study of how the activation area and strength changes for different acceleration factors will be made with an incomplete performed task.

2 THEORY

2.1 Functional magnetic resonance imaging

Functional magnetic resonance imaging (fMRI) is a method using magnetic resonance to image functional areas in the brain. A common method is using the blood oxygen level as a measure of the neuronal activity while different tasks are performed, to get measurable activations.

2.1.1 Blood oxygenation level dependent fMRI (BOLD)

BOLD-fMRI is a conventional fMRI method which uses the blood oxygenation level to measure activation. Stimulation of neurons leads to an increase in synaptic activity which leads to a local increase in energy and oxygen consumption. This in turn leads to a local increase in bloodflow. The vascular system supplies the brain with energy in form of glucose and oxygen, where oxygen is transported bound to haemoglobin. The arteries transport the oxygenated blood trough increasingly smaller vessels to the capillaries where the oxygen is transferred to the neurons [7]. Because there is an overshot in blood flow compared with the oxygen metabolism, the ratio between oxygenated blood in the arteries and deoxygenated blood in the veins will increase [2]. BOLD-fMRI uses the difference in magnetic susceptibility between oxygenated and deoxygenated blood to create image contrast [8]. Blood consists mostly of haemoglobin. Deoxygenated haemoglobin is paramagnetic while oxygenated is diamagnetic. Differences in oxygen levels therefore lead to different local distortions in the magnetic field. This leads to different T2*-relaxation which varies exponentially with the concentration of deoxygenated blood [7]. Since the difference in T2* is being measured, a gradient echo pulse sequence is suitable for fMRI.

The BOLD haemodynamic response describes the signal intensity change over time after and during stimulation. When the stimuli starts there is initially a small decrease in intensity which is caused by a change in the metabolism before the initiation of the haemodynamic response. The haemodynamic response then causes a signal increase which in longer stimulation often rises to a higher value before it reaches a plateau. This is called overshooting. In order to detect the small signal change over the background noise an averaging over time is made. A model, which describes how the BOLD signal varies with the stimuli, is built to which the random error is added to explain why the observations varies even if the same experiment is repeated. A commonly used model is the general linear model and can be seen in equation (2). The haemodynamic response model is called the haemodynamic response function (h(t)) [7]. A paradigm describes the distribution of stimulus over time. There are two designs of paradigms, event related and block related. In block design, blocks of stimuli versus blocks of rest is used. A more complex design is the event-related design where stimuli is presented randomly. Because it gives a subjective response, it is often used to study the behaviour of the subject [9]. To get the BOLD response x(t), the haemodynamic response function is convolved with the modelled stimuli, which can be seen in Figure 1. The haemodynamic response function can be modelled in different ways, one example can be seen in equation (1) [7].

$$h(t) = \left(\frac{t}{a_1}\right)^{d_1} exp\left(\frac{-(t-d_1)}{b_1}\right) - c\left(\frac{t}{d_2}\right)^{a_2} exp\left(\frac{-(t-d_2)}{b_2}\right) \tag{1}$$

where $d_j = b_j a_j$ is the time to the peak and t is time.

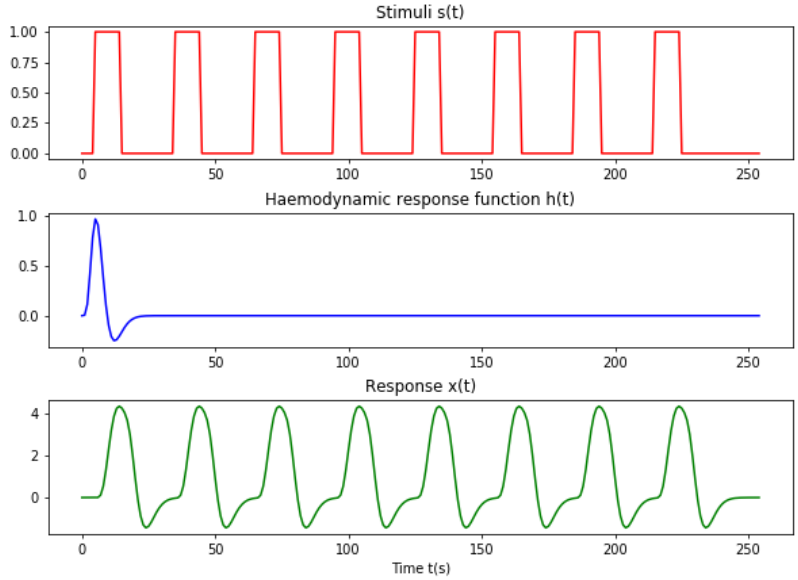

Figure 1: Stimuli with a block design as a function of time, the hemodynamic response function and the stimuli convoluted with the hemodynamic response function which gives the response function.

2.1.2 General linear model

The general linear model is a function which, when used in fMRI analysis, models how the signal should change during a paradigm. The acquired data is fitted to the model to determine how well the data is explained by the model. The general linear model can be seen in equation (2).

$$y_i = x_{i1}\beta_1 + ... + x_{im}\beta_m + \varepsilon_i \tag{2}$$

which in matrix form can be written as in equation (3)

$$\mathbf{Y} = \mathbf{X}\beta + \varepsilon \tag{3}$$

where Y are the measured values, X is the BOLD response model, β is the response magnitude where magnitudes from different stimulus are added together and ε is the error [7]. In fMRI, the time series are correlated in time and will affect the result by a decrease in the degree of freedom [10]. This correlation has to be taken into account when the repetition time is less than approximately 4 s [5]. This is called temporal autocorrelation and has to be added to the error to be able to do a correct error estimation and in turn be able to detect

the presence of a BOLD signal. The error term consists of both white noise from the scanner and physiological coloured noise and can be described with equation (4).

$$\varepsilon_i = \eta_i + \chi_{i2} \tag{4}$$

$$\eta_i = \rho\eta_{n-i} + \chi_{i1} \tag{5}$$

where η_i is coloured physiological noise and accounts for the temporal autocorrelation, χ_{i1} is the white noise and χ_{i2} is white noise originating from the scanner [7]. Due to the temporal autocorrelation, the increase in statistical power will not be the square root of the multi-band acceleration factor. It will instead be both dependent on the increase in amount of data sampled and the temporal autocorrelation [5].

The β-values in equation (3) are a measure of how strongly the data fits the model where large values indicate a good fit. To estimate β-values, the values of β, which minimise the sum of square errors, are determined. This can be done using the least square fit. To be able to determine if the signal change between rest and stimuli is significant, a contrast vector c', which has the same length as the $\hat{\beta}$ vector, is used. The contrast vector is often represented by 1 for stimuli and 0 for rest which gives different β-values different weighting factors. The effect is then given by $c'\hat{\beta}$. A T-test can for example be used to determine whether the difference in signal is statistically significant (see equation (6)) [7].

$$T = \frac{c'\hat{\beta}}{V\hat{a}r(c'\hat{\beta})} \tag{6}$$

where $V\hat{a}r(c'\hat{\beta})$ is the variance of the effect.

2.1.3 Limitations of fMRI in intra-subject studies

There are several limitations when performing fMRI studies within individuals and sessions. Limitations such as noise from the scanner, artifacts and drifts are unavoidable but also possible to correct for [11].

Motion of the subject's head can lead to a decrease in image quality and is important to correct for to ensure reliability. Analysis methods for fMRI assume that the same anatomical brain location corresponds to the same voxel for all repetitions, which if there is head motion, would not be true. Head motion also changes the local magnetic field, which leads a change in $T2^*$ and therefore intensity variations in the images [12]. Signal variations can also arise due to so-called spin history effects. These effects arise from non-homogeneous excitation profiles throughout the object, and if the spin system has not return to equilibrium before next excitation pulse the magnetic state of the system will depend on the previous magnetic states. If head movement occurs between two excitation pulses, it can lead to spin history related image artifacts. [13]. Because head motion has a large impact on the data, a restriction of the translational movement is often set to 1 mm and the rotational movement to 1 degree for images with resolution 2-3 mm [12, 14]. Artifacts due to head motion can

occur with motions as small as a few tenths of millimetres between consecutive frames [11].

There are also physiological variations which can affect the reliability when doing intra-subject comparisons. Both breathing and heart rate will affect the fMRI measurements where breathing will lead to magnetic field changes due to respiratory motion and different breathing rate and depth will lead to different amounts of CO2 concentration and different blood flow. Heart rate will affect the fMRI measurement as the pulsating blood will give fluctuations in the signal intensity. The vasomotion, which is spontaneous oscillation in the blood vessels, can also affect the measurements by adding low frequency ocillations to the BOLD-singal [11].

2.2 Preprocessing of data

Before the raw data can be analysed for activation, preparations of the data have to be made. Preprocessing of the data helps reduce errors and makes the result of the statistically analysed activations in the brain valid [7].

Motion during scanning is one of the most important factors which can affect data quality [14]. This can lead to false areas with activation and it is important that each voxel corresponds to the same anatomical point in every time series. Therefore, an estimation of motion has to be made and corrected for. This can be done in several different ways but is a time consuming process. To reduce the processing time, a rigid body is often assumed. This means that the shape of the head and brain is assumed to be constant [7]. In the rigid body model, six parameters describe the volume transformation. Three rotations and three translations directions are then called six degrees of freedom [14]. The motion correction can be made by matching volumes to for example the first volume where the image can be shifted or rotated along and around the x,y and z axis [7].

Spatial filtering is used as a preprosessing step to reduce noise, hence increasing the signal to noise ratio. To peform spatial filtering, a convolution with a Gaussian profile on each image can be made. The FWHM determines the amount of filtering and is often between three to ten mm [7].

In fMRI analysis the model assumes that all the time points in a voxels time series are sampled at the same time. This makes the model fitting not optimal and the voxels must therefore be adjusted so that they seem to be sampled at the same time. This is called slice time correction and is made by adding a phase shift, often in the frequency domain [7].

Temporal filtering is applied in every voxel's time series separately and is used to remove, compared with the activation, lower frequencies. These frequencies originate from slowly varying psychological effects and from drifts in the scanner. If slow varying frequencies are not removed , they can contribute to the noise in later statistical analyses. If the lower frequencies are not correlated to the stimuli, the fitting to the model will improve if the frequencies are removed. To filter out lower frequencies a high-pass, butterworth filter can be applied [7].

Coregistration is important in fMRI imaging because time-dependent changes are studied, and if intersubject studies are made, a transformation to a standard space also has to be done. Spatial transformation can be divided into label based and non-label based transformations, and can be made linear or non-linear. In label based transformations, spatial structures or landmarks are identified. The transformation that best, based on the labels, superimpose the images is used. In non-label based transformation, differences between the object and reference image are minimised. [15]

2.3 Multiband EPI

EPI (echo planar imaging) is a technique where the whole k-space is sampled after one RF excitation pulse. This makes it a fast pulse sequence and is therefore suitable for fMRI. The sampling time can be be reduced even further by exciting and imaging several slices simultaneously, alternatively sample more data at the same time as for traditional EPI. This technique has shown to be suitable when the simultaneous excited slices are well separated [16]. Therefore the simultaneously excited slices are often chosen to be separated with a distance as large as possible and the separation will be dependent on the acceleration factor. The pulse sequence can be seen in Figure 2 and shows a pulse sequence with acceleration factor three. This means three different slices are excited and imaged at the same time and are, in Figure 2, displayed with different colours.

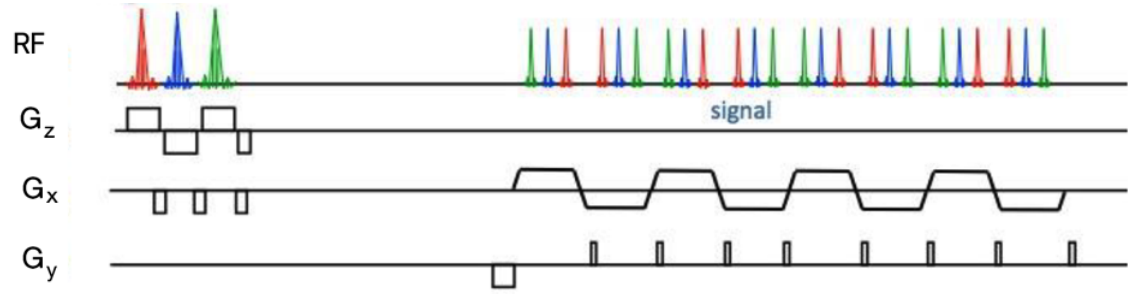

Figure 2: A multiband EPI pulse sequence where the red, blue and green are three different RF excitations pulses and echoes and G_z is the slice selective gradient, G_x is the frequency-encoding gradient and G_y is the phase-encoding gradient. Adapted from [17].

There are also disadvantages with the multiband EPI pulse sequence. The temporal signal to noise ratio is dependent on the acceleration factor where a higher acceleration will result in a decrease. This is due to both a shorter repetition time, which means a decrease in the steady state longitudinal magnetisation, and an increase in the g-factor noise where the g-factor is noise originating from reconstruction of the superimposed signals. The steady state longitudinal magnetisation will in turn be dependent on the $B1^+$ field, and the longitudinal T1 relaxation time [5]. Where the $B1^+$ field is the transmitted radio-frequency field [18].

The g-factor noise appears from reconstruction of the slice-aliased data, and is commonly used to measure quality in fMRI images. The g-factor will be both spatially non-uniform

and subject specific. This is due to its dependency on both parameters related to the SMS-sequence like slice position, SMS-acceleration, the in-plane acceleration and the caipirinha-shift and to geometric parameters like the dimensions of the brain and the receiver coil array [5].

2.3.1 Multiband waveform

The RF pulse needed for excitation of a slice can be described with equation (7) and seen in Figure 3 (top).

$$RF(t) = A(t) \cdot P(t) \tag{7}$$

where $A(t)$ is the standard complex RF waveform that determines the slice profile together with the slice selective gradient and $P(t)$ modulates the phase to determine the slice position. The phase modulation function can be seen in equation (8).

$$P(t) = e^{\Delta\omega t + \varphi} \tag{8}$$

Where $\Delta\omega$ is the slice position and φ is the phase when TE is zero. An RF pulse that excites multiple slices can be created by superposition of several RF wave forms. This can be seen in equation (9).

$$RF_{MB}(t) = A(t) \sum_{N} e^{\Delta\omega_n t + \varphi_n} \tag{9}$$

Often, the same waveform and flip angle are used for all slices and $A(t)$ can therefore be placed outside the summation. One problem with the design of the multiband RF pulse is that there is a risk of exceeding the peak amplitude capabilities of the amplifier and the SAR limit as the number of simultaneously excited slices increases. Multiband waveform is a linear superposition of several single band wave forms and the peak RF voltage will therefore increase linearly with number of simultaneous excited slices [19]. A solution to reduce the peak amplitude is to use power independent number of slices (PINS). In this technique, a single band wave form is undersampled and split into discrete subpulses which gives a periodic excitation in the slice selection direction [20]. A PINS-pulse can be seen in Figure 3 (bottom). For the same number of slices, this technique gives an approximate number of N in lower peak RF power, where N is number of simultaneous excited slices [19]. Together with the PINS-pulse a blipped slice selection gradient is used which is switched on and off and is interleaved with the PINS-pulse [20].

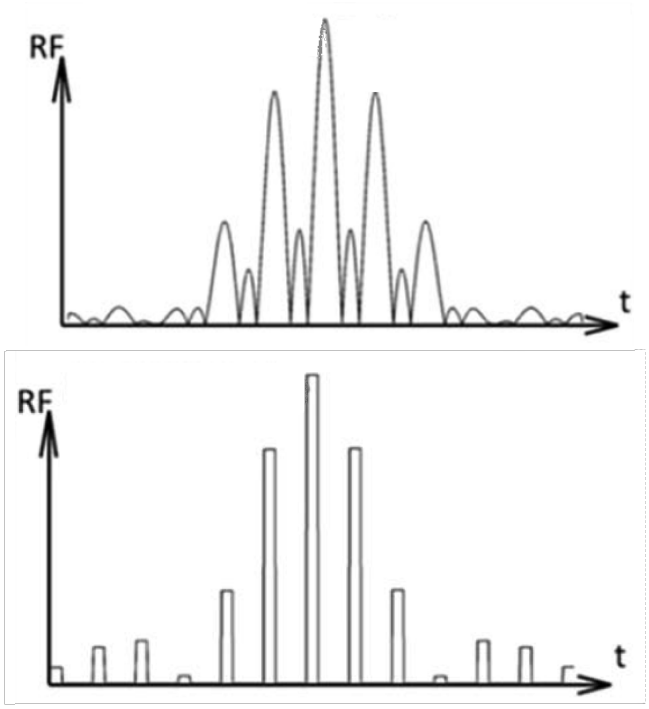

Figure 3: Multiband RF-pulse and a PINS pulse created by undersample and split a single band pulse into discrete subpulse. Adapted from [21].

2.3.2 CAIPRIHINIA

Parallel imaging is a technique used to shorten the acquisition time and can be done by skipping lines in the phase encoding direction. This leads to an under sampled k-space and aliasing artifacts. To avoid artifacts, coil encoding, which uses the sensitivity of the multi coil receiver array can be applied. When the spatial sensitivity of the multi coil array is not sufficient, a combination of coil encoding and phase encoding can be used. With phase encoding, different slices receive different phases which modifies the appearance of the artifacts. When using multi slice techniques, several slices are excited at the same time. This means that signal from the same position in the phase and frequency encoding direction, but from different slices, will be superimposed. To receive a spatial resolution in the slice direction the same methods as for parallel imaging can be used. Caipirinha is a method which shifts slices in relation to each other in the FOV with phase encoding. This make the former aliased pixels originate from different locations in the FOV and therefore makes it possible to separate them. This methods gives a reduction in the noise coming from the untangling of signals [4]. Example of an EPI pulse sequence with blipped Caipirinha can be seen in Figure 4.

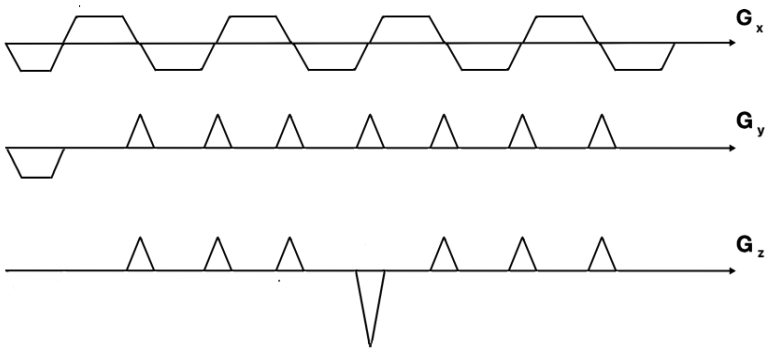

Figure 4: EPI pulse sequence with blipped caipirinha, creating a FOV/4 shift in the slice encoding direction, G_z. The blipps can be seen in the phase encoding direction, G_y

2.3.3 Reconstruction methods

To reconstruct data acquired with the Caipirinha technique, slice-GRAPPA can be used. Slice GRAPPA is based on GRAPPA but is slice specific [21]. GRAPPA is a method which uses the center of a fully sampled low resolution k-space to create a kernel (K) with weighting factors, which describes the sensitivity of the different coils through the FOV. These are called auto calibration signals (ACS). The acquired data points are fitted to the ACS line where data from all coil element are used to fit a single ACS line in a single element. This can be seen in Figure 5. The missing datapoints are then reconstructed using the neighbouring data points and a kernel, consisting of weighting factors from the fitting of the ACS line. Convolution is made in the k-space and creates one image for each coil which then are combined using a normal sum of squares reconstruction [22]. In slice-GRAPPA there are slice specific weights instead, which gives a specific kernel for each slice. The fitting procedure in slice GRAPPA produce kernels which minimize the image artifacts. Split slice-GRAPPA is a method to reduce signal leakage between slices. It uses that leakage can be derived from the slice specific weight and can therefore be used to cancel the signals coming from another slice [21]. Split slice GRAPPA kernel, unlike the slice GRAPPA method, both tries to minimise the slice leakage and the image artifacts [16].

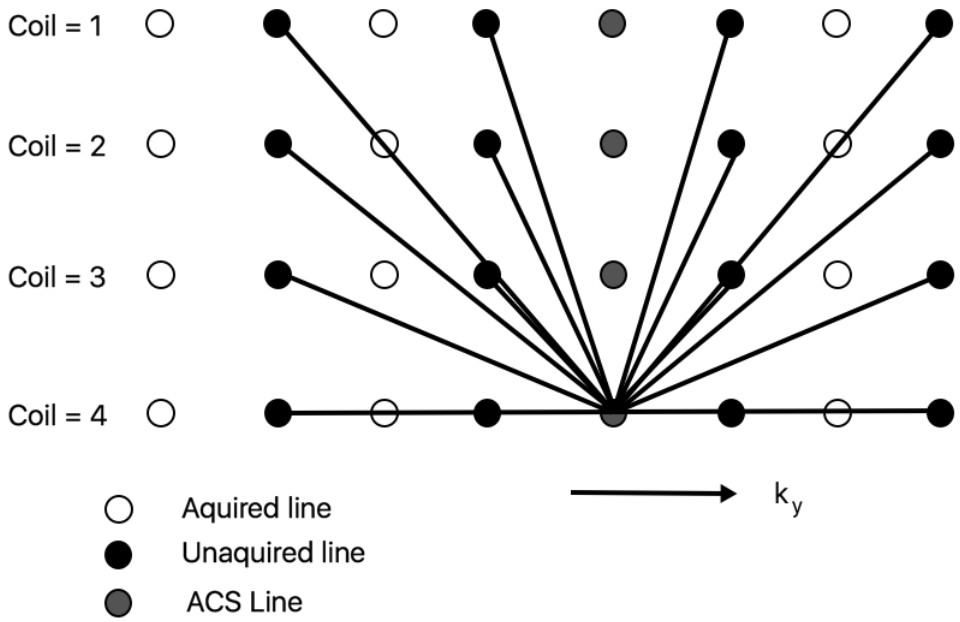

Figure 5: GRAPPA reconstruction method, where acquired data from every coil is fitted to the single ACS line.

2.4 Artifacts in Multiband EPI data

When several slices are simultaneous excited, signal leakage to a neighbouring slice can occur. This is called slice leakage and can lead to false positive activations and can therefore have a large impact on the fMRI data. To reduce this effect, different reconstruction methods can be used where one commonly used is split slice GRAPPA [16].

In EPI images the complete 2D-space is sampled in one excitation with an oscillating readout gradient. Because of the alternation, half of the sampled k-space lines have to be time-reversed before fourier transformation. If there is an inconsistency between the two different readout directions, ghost projections of the image with half of the FOV will appear. This causes artifacts called N/2 ghosts or Nyquist ghosts, see Figure 6. The inconsistency can occur due to eddy currents and off resonance shifts and can be a concern in fMRI if a BOLD activated region creates a N/2 ghost artifact with an intensity that can be mistaken for false activation [23].

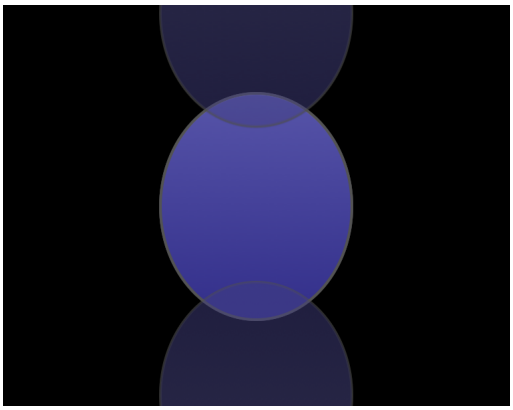

Figure 6: Schematic example of ghosting artifact with N/2 shift. Duplicates with lower intensity can be seen with a displacement of half the FOV in the phase encoding direction.

2.5 Image quality measurement

To determine image quality, there are several different parameters that can be used. One parameter that is important in fMRI is the temporal signal to noise ratio (tSNR) which describes the signal to noise ratio over time. The tSNR can be calculated by taking the mean signal for all voxels over time divided by the standard deviation according to equation (10).

$$tSNR = \frac{\bar{m}}{\sigma} \tag{10}$$

where $\bar{m}$ is the mean signal over time and σ is the standard deviation over time. Equation (10) can be used to calculate tSNR-maps where the equation is applied for all voxels time series [6].

The g-factor can be calculated using equation (11).

$$g_{app} = \frac{tSNR_{full}}{tSNR_{acc}} \tag{11}$$

where g_{app} is the apperent g-factor, $tSNR_{full}$ is the tSNR in the fully sampled image and $tSNR_{acc}$ is the tSNR in the accelerated image [24].

3 MATERIAL AND METHOD

3.1 Phantom measurements

All measurements were performed on a Siemens Prisma 3T (Erlangen, Germany) using a cylindrical water phantom. For the phantom measurements, the standard EPI pulse sequence and the Multiband EPI pulse sequence with acceleration factors 2, 3, 4, 6, and 8 were used (see Table 1). Furthermore, unaccelerated multiband EPI pulse sequence was used. All functional volumes had a resolution of 3x3x3 mm^3, a 30 ms echo time, 100 number of measurements and consisted of 36 slices. For every pulse sequence the repetition time was set as low as possible. Measurements were performed using three different head coils, 20, 32 and 64 respectively. Flip angle was calculated using the Ernst angle. In the phantom measurements, the number of volumes were constant for all pulse sequences i.e., varying acquisition time depending on the acceleration factor. Parallel imaging with acceleration factor 2 was used in the phase encoding direction for all pulse sequences and the reconstruction method used was split slice GRAPPA.

Table 1: Repetition time and flip angle for all acceleration factors.

Acc factor	TR[ms]	FA [^{o}]
0	2860	87
2	1020	69
3	686	60
4	520	54
6	357	46
8	301	42

3.1.1 Evaluation of phantom images

To evaluate the water phantom data, temporal signal to noise ratio was calculated using equation (10) for every voxel in the volume, which gave tSNR-maps. The g-factor was calculated using equation (11) for all voxels creating g-maps. Before the g-factor was calculated, a mask was made to cancel out the background. Histograms over the tSNR-maps were calculated for the whole volume. All calculations and visualisations were implemented using Python.

3.2 Volunteer measurements

Measurements were carried out on ten healthy volunteers. Pulse sequences used were the standard EPI sequence and the multiband EPI sequence with acceleration factors 2, 3, 4 and 6 (see Table 2). All functional volumes had a spatial resolution of 3x3x3 mm^3 and consisted of 36 slices. A 30 ms echo time was used for all acquisitions. Image acquisition time was set to 3.36 min matching the standard clinical fMRI protocol for all pulse sequences which gave different number of measurements for the different acceleration factors. Every

pulse sequence was sampled with both the 20 channel coil and the 64 channel coil chosen based on the phantom measurements. In order to keep a reasonable total scan time, the 32 channel coil was excluded from the volunteer experiments. Finger tapping was used in the paradigm and performed with the right hand which gave activation in, among other areas, motor cortex and somatosensory cortex. The paradigm consisted of blocks of 20 s finger tapping and 20 s rest. Each block of work and rest was repeated 5 times. A high resolution MPRAGE volume was acquired for both coils with the resolution 1x1x1 mm^3. Between the measurements with the 20 channel coil and the 64 channel coil, a rest for approximately five minutes was obligatory. Caipirinha was used with different shifts dependent on the acceleration factor, where the different shifts can be seen in Table 2. The shifts were given by the manufacturer, although no information regarding the shift for acceleration factor 6 was available. The reconstruction method used was split slice GRAPPA. For subject 2, the only high resolution volume acquired was with the 20 channel head coil because of problems with the MR-scanner. For subject 8, the unaccelerated volume acquired with the 20 channel head coil had to be excluded because of unreasonable low activation compared with the accelerated volumes for the same volunteer.

Table 2: Repetition time, flip angle, number of measurements for all acceleration factors. The Caipirinha shift can be seen for the accelerated volumes except for acceleration factor 6.

Acc factor]	TR[ms]	FA[°]	number of measurements	Caipirinha shift
0	2860	87	72	-
2	1020	69	205	8
3	686	60	302	6
4	520	54	399	6
6	357	46	580	-

3.2.1 fMRI analysis

All fMRI analysis were performed using FSL [25]. Before doing the fMRI analysis, a brain extraction was made. In the analysis, a threshold for the z-values was set to 3.1 and a high pass filter with a 90 s cutoff and a spatial filter with a FWHM off 6.0 mm was used. A motion correction was made by applying a rigid-body transformation. Registration to standard space was made on the high resolution volume. The MNI152 standard-space T1-weighted average structural template volume [26] with resolution 1x1x1 mm was used for the registration. A GLM model was set up where the first 6 s in the paradigm were skipped, on and off and phase was set to 20 s each and convolution was made with a Double-Gamma HRF function. The contrast vector was set to $c = [1, 0]$. The statistical volume was then registered to the high resolution standard space with the same transform as was used for the high resolution volume registration.

3.2.2 Evaluation of volunteer data

A mask was made based on the finger tapping activation area and was made by segmenting the motor cortex and primary somatosensory cortex. The segmentation was made on the high resolution volumes registered to standard space were the Juelish atlas [27, 28] was used to extract the functional areas. By using the volume registered to the standard space, the same mask could be used for all subjects. The mask was applied to all volumes. Number of voxels with t-values higher than a threshold, number of voxels with the highest 10% t-values and mean value of the 10 % highest t-value in the volume were determined. All evaluations were performed using Python.

For all above mentioned parameters, the difference between the accelerated volumes and the unaccelerated volume was calculated, and a paired two-tailed t-test was made to determine if the difference was significantly different from zero. Subject motion was examined to estimate the displacement for each volume acquisition. Both the mean value of the absolute displacement and the relative displacement were evaluated.

3.2.3 Study with an incomplete paradigm

As a complementary experiment, an investigation of the effect of multiband acceleration in a clinically feasible case of a non-compliant patient was made. The difference in activation between a correct performed paradigm and an incomplete performed paradigm was examined. This study was based on result from the previous volunteer measurements. Volumes were acquired with the standard EPI pulse sequence and with the multiband EPI pulse sequences with acceleration factors 2, 3, 4 and 6. The 64 channel head coil was used for all pulse sequences. Same parameters as in Table 2 were used and number of imaged slices was 36. All volumes were sampled twice. One with the finger tapping paradigm as previous and one where two blocks with finger tapping were skipped. The EPI volumes were analysed, as previously described, using FSL [25].

The differences and relative difference between the volumes with the correct performed paradigm and the volumes with the incomplete paradigm were calculated where the number of voxels with t-values higher than 3.1 and the highest t-values were evaluated.

4 RESULT

4.1 Phantom measurements

The tSNR decreased with the acceleration factor for all the head coils, however higher tSNR values were observed in the 32 and 64 channel head coil than the 20 channel head coil. A higher tSNR could also be seen in the outer parts of the phantom compared with the center. Artefacts were more prominent for higher acceleration factors and for the 20 channel head coil. One slice from the tSNR- map can be seen in Figure 7 (left panel) for the 20, 32 and 64 channel head coils for the standard EPI volume, the unaccelerated volume with the multiband pulse sequence and the accelerated volumes with acceleration factors 2, 3, 4, 6 and 8 using the multiband EPI pulse sequence. All volumes acquired with same head coil display the same slice in the water phantom.

For the higher acceleration factors, an increase in g-factor noise was seen, with a more prominent difference in the 20 channel head coil. In the g-maps, an increase in artifacts was seen for the higher acceleration factors as well. The g-maps can be seen in 7 (right panel).

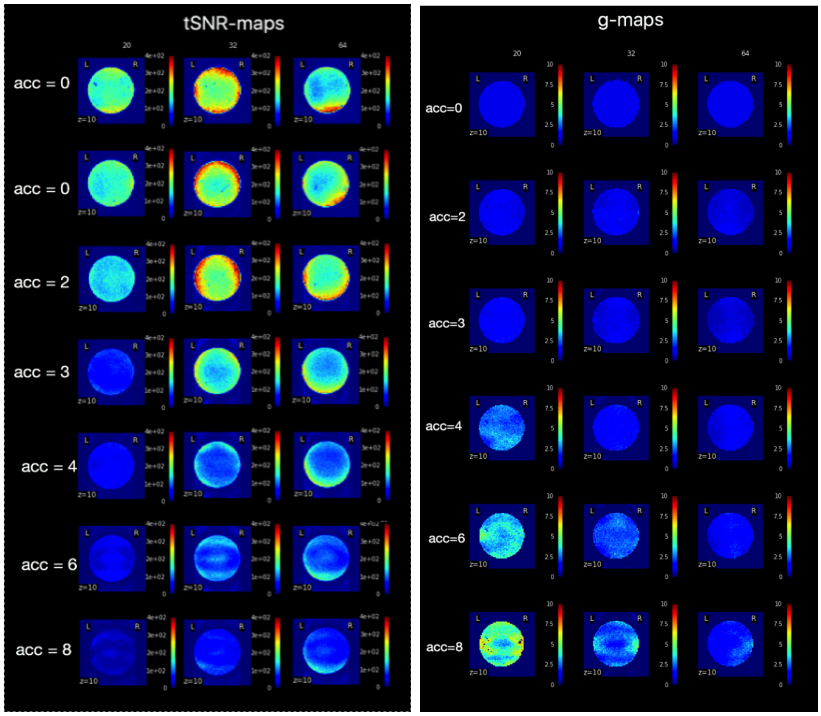

Figure 7: Phantom measurements with the 20 channel head coil, 32 channel head coil and 64 channel head coil. At the top, one slice from the standard EPI volume can be seen, then a slice from the unaccelerated volume acquired with the multiband EPI pulse sequence and slices from volumes with the different acceleration factors 2, 3, 4, 6 and 8.

Histogram over the whole volume for the different coils can be seen in Figure 8. The tSNR-values were displaced towards higher t-values for the lower acceleration factors and there was a more pronounced difference between the acceleration factors for the 32 and 64 channel

coil than the 20 channel coil. The 20 channel coil had a higher number of lower tSNR-values for all acceleration factors compared with the two other coils.

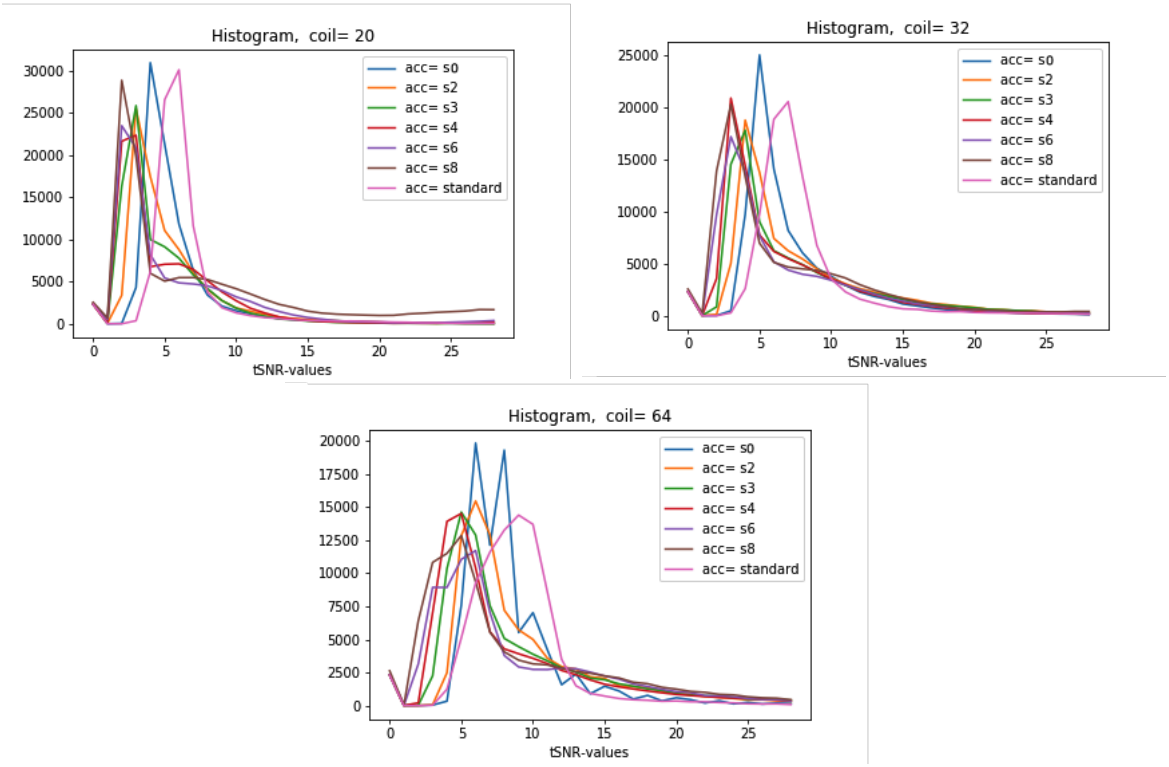

Figure 8: Histogram over the whole volume from the phantom measurements with the 20 channel head coil, 32 channel head coil and 64 channel head coil. Slices are from volumes acquired with the multiband EPI pulse sequence with acceleration factors 0, 2, 3, 4, 6 and 8 and from the volume acquired with the standard EPI pulse sequence.

4.2 Volunteer measurements

The motion parameters were evaluated for all volunteers. Both the mean relative displacement, the motion between two consecutive time points and the absolute displacement, the displacement between a time point and a reference point. The translation movements were below 1 mm and the rotational movements below 1 degree for all volunteers as can be seen in Figure 17 and 18.

4.2.1 Example images of one volunteer

An increase in noise level was seen in the higher acceleration factors, where higher noise was observed in the 20 channel head coil. A higher signal was seen in the edges of the head compared with the center, where the difference was more pronounced in the 64 channel head coil. In Figure 9, one slice from each EPI-volume, the unaccelerated and accelerated ones, for one volunteer can be seen for both the 20 channel head coil and the 64 channel head coil.

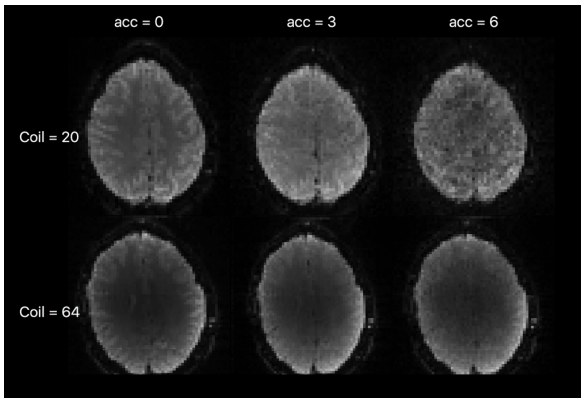

Figure 9: Example of a slices from the EPI-volume and slices from the multiband EPI-volumes selected from one volunteer. The Figure is showing an unaccelerated slice and slices with the different acceleration factors 3 and 6 for both the 20 channel head coil and the 64 channel head coil.

Highest tSNR-values was observed in the unaccelerated volumes for both head coils but were relatively constant between the unaccelerated volume and acceleration factor 2 in the 64 channel head coil. Higher tSNR was also seen in the outer part of the head. An overall higher tSNR could be seen in the 64 channel head coil. Figure 10 shows a slice from the tSNR-maps calculated from the unaccelerated volume and volumes with acceleration factors 2, 3, 4 and 6 for one volunteer. Slices can be seen both for the 20 channel head coil and the 64 channel head coil.

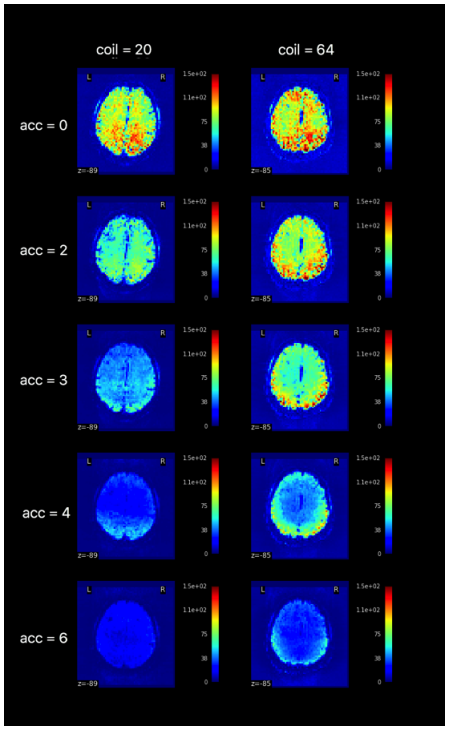

Figure 10: Example of a slices from an unaccelerated volume and accelerated volumes acquired with acceleration factors 3, 4 and 6 showing the tSNR for for both the 20 channel head coil and the 64 channel head coil.

Figure 11 shows example images of a slice from the unaccelerated volume acquired with the EPI pulse sequence and from the accelerated volumes acquired with the multiband EPI pulse sequence for 20 -and 64 channel coils. The statistical maps are displayed on top of the high resolution slice acquired with the same head coil. Both the statistical maps and the high resolution volumes were registered to the standard volume. The slice is same for all acquired with the same coil and chosen because it contains a highly activated area. The t-values threshold was set to 3.1 for all slices. Note the spurious activations in the slices acquired with lower acceleration factors.

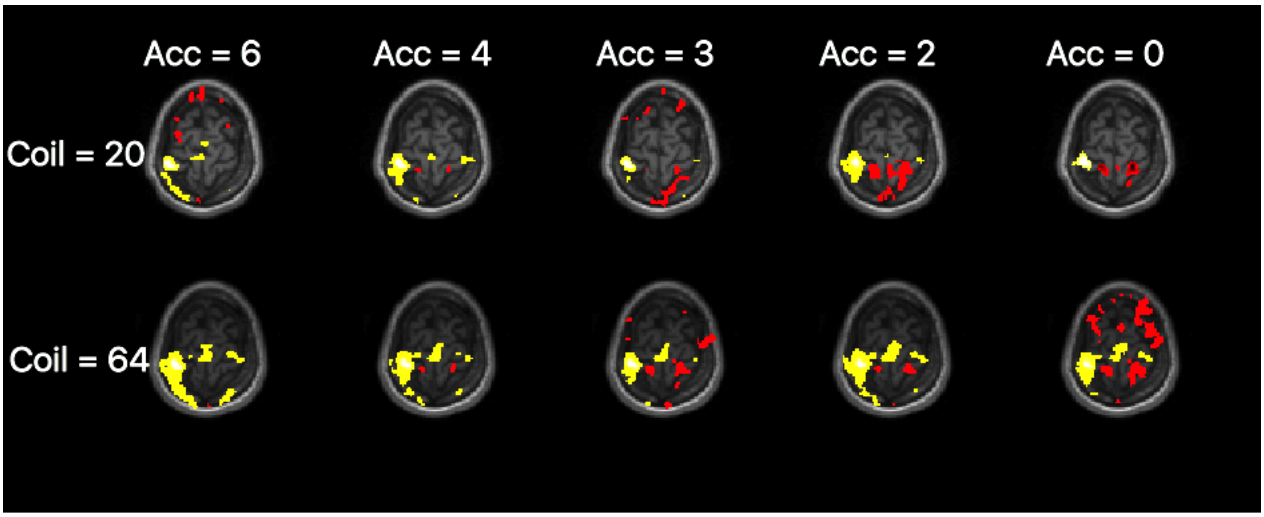

Figure 11: Example images from one volunteer showing a slice in the unaccelerated volume and volumes acquired with the different acceleration factors 3, 4 and 6 for both the 20 channel head coil and the 64 channel head coil.

4.2.2 Evaluation of volunteer data

Three parameters were studied as both mean values for the volunteers and as mean differences between the accelerated volumes and the unaccelerated volume: number of voxels with t-values higher than 3.1, the mean 10% highest t-values and number of voxels with the 10% highest t-vales. It is displayed in both figures and tables. Data-points had to be excluded and are denoted in the tables.

The mean values of number of voxels with t-values higher than 3.1 for all volunteers decreased with the acceleration factor for the 20 channel head coil. For the 64 channel head coil, the mean value increased for acceleration factor 2, 3 and 4 and decreased for acceleration factor 6 compared with the unaccelerated volume. This can be seen in Figure 12 (left) and can also be observed in Figure 12 (right) where the mean difference in number of voxels with t-values higher than 3.1 between the unaccelerated volume and the unaccelerated volumes was below zero for all acceleration factors acquired with the 20 channel head coil. The difference was greater than zero for acceleration factor 2 and 3 for the 64 channel head coil, and below zero for acceleration factor 4 and 6. The difference was significant with $p < 0.01$ for acceleration

factor 2 with the 64 channel head coil. This can also be seen in Table 3 together with the standard errors and p-values. High standard deviations were also observed in the Figure, more notably for the unaccelerated volume acquired with the 20 channel head coil.

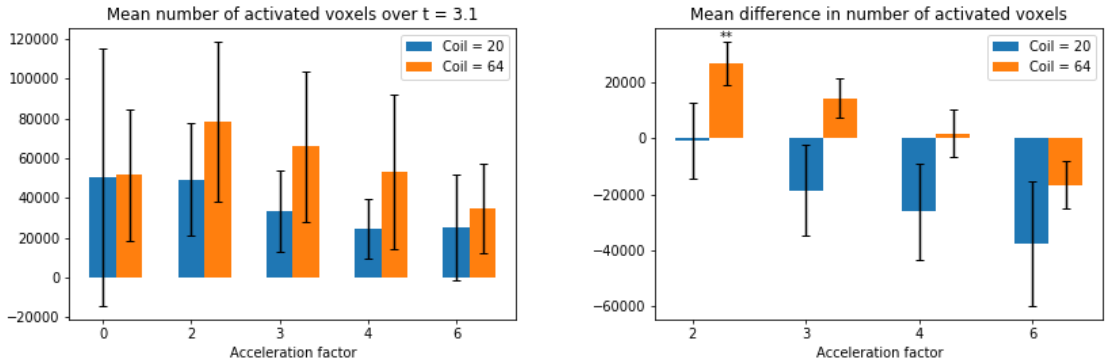

Figure 12: Mean value of number of voxels with t-values above 3.1 for all volunteers (left), both for the 20 channel head coil and the 64 channel head coil and the mean difference between the accelerated volumes and the unaccelerated volume (right). The difference is significant for acceleration factor 2 with $p < 0.01$.

In Table 3 the mean value of number of voxels with t-values higher than 3.1 and mean difference between the unaccelerated volume and the accelerated volumes and the standard error for all volunteers can be seen. The Table displays values for both the 20 channel and the 64 channel head coil, where the mean difference was significant with $p < 0.05$ for acceleration factor 2 with the 64 channel coil. Number of voxels where higher for the accelerated volume.

Table 3: Mean value of number of voxels with t-values higher than 3.1, the mean difference between the accelerated volumes and unaccelerated volume for the volunteers, the standard error of the difference and the p-value calculated from a paired two-tailed t-test. Significant values can be seen in bold.

Acc. factor	Head Coil	mean value	mean difference	standard error	p-value
0	64	51684	-	-	-
2	64	78661	26978	8178	**0.009**
3	64	65977	14293	7451	0.087
4	64	53480	1796	9056	0.847
6	64	34977	-16707	8949	0.095
0	20	50513^{+}	-	-	-
2	20	49671^{+}	-841	13014	0.780
3	20	31787^{+}	-18725	17237	0.309
4	20	24357^{+}	-26155	18147	0.181
6	20	$16096^{+\diamond}$	-34417	27287	0.330

$^{+}$ Value for subject 6 excluded

$^{\diamond}$ Value for subject 1 excluded

The mean value of the mean 10% highest t-values was slightly increased for higher acceleration factors in the 64 channel head coil but decreased in the 20 channel head coil, with the exception of acceleration factor 2. This can be seen in Figure 13 (left) which shows the mean value for the unaccelerated volume and the accelerated volumes for both head coils. The mean difference in the mean 10% highest t-value was above zero for acceleration factor 2 with $p < 0.01$ and below zero for acceleration factor 3, 4 and 6. This for the 20 channel head coil. For the 64 channel head coil the difference was above zero for all acceleration factors with $p < 0.01$ for acceleration factor 2 and $p < 0.05$ for acceleration factor 4. This is displayed in Figure 13 (right) and can also be seen in Table 4 together with the standard errors and p-values.

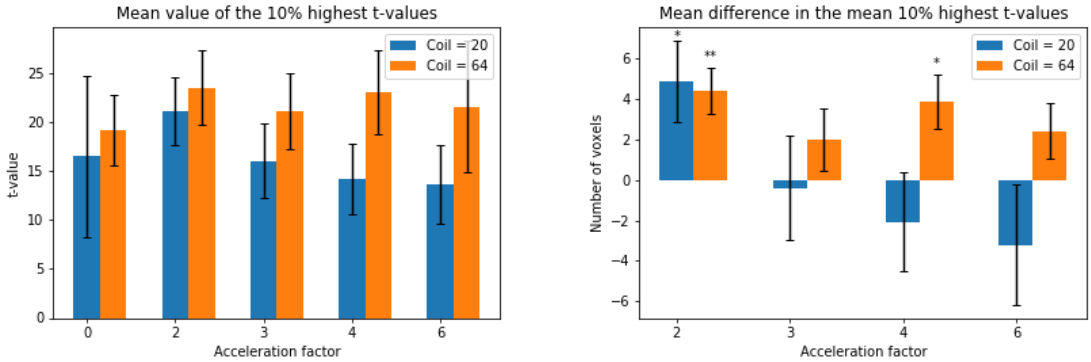

Figure 13: Mean value for the volunteers of the mean 10 % highest t-values (left) and the mean difference between the accelerated volumes and the unaccelerated volume (right) for both the 64 channel head coil and the 20 channel head coil. Significance can be seen for acceleration factor 2 with $p < 0.05$ in the 20 channel head coil and factor 2 and 4 with $p < 0.01$ and $p < 0.05$ respectively in the 64 channel head coil (right).

The mean difference in the mean 10 % highest t-values between the unaccelerated volume and the accelerated volumes for the 64 channel head coil showed a significance with $p < 0.01$ for acceleration factor 2 and $p < 0.05$ for acceleration factor 4. The t-values were higher for the accelerated volumes. For the 20 channel head coil the difference was significant for acceleration factor 2 with $p < 0.05$ where a higher value was observed in the accelerated volume. This can be seen in Table 4.

Table 4: Mean 10 % highest t-values for the volunteers, the mean difference between the accelerated volumes and unaccelerated volume, the standard error of the difference and the p-value calculated from a paired two-tailed t-test, where significant values can be seen in bold.

Acc factor	HeadCoil	mean value	mean difference	standard error	p-value
0	64	19.2	-	-	-
2	64	23.6	4.4	1.1	**0.004**
3	64	21.2	2.0	1.6	0.236
4	64	23.1	3.9	1.3	**0.017**
6	64	21.6	2.4	1.4	0.116
0	20^{+}	16.5	-	-	-
2	20^{+}	21.4	4.9	2.0	**0.038**
3	20^{+}	16.1	-0.4	2.5	0.878
4	20^{+}	14.4	-2.1	2.4	0.417
6	$20^{+\diamond}$	13.1	-3.4	2.9	0.305

$^{+}$ Value for subject 6 excluded

$^{\diamond}$ Value for subject 1 excluded

For the 20 channel head coil, highest mean value of number of voxels with the 10% highest t-values was obtained for the unaccelerated volume and lowest for the volume acquired with acceleration factor 6. For the 64 channel head coil, acceleration factor 3 gave a slightly higher number of voxels, but the values were relatively similar for all acceleration factors. Figure 14 (left) shows the mean values both for the 20 and 64 channel head coil. The mean difference in number of voxels with the 10% highest t-values between the unaccelerated volume and the accelerated volumes was below zero for all acceleration factors with $p < 0.01$ for the 20 channel head coil. For the 64 channel head coil the difference was above zero for acceleration factor 3, around zero for acceleration factor 2 and 4 and below zero for acceleration factor 6. The mean difference can be seen in Figure **??** (right).

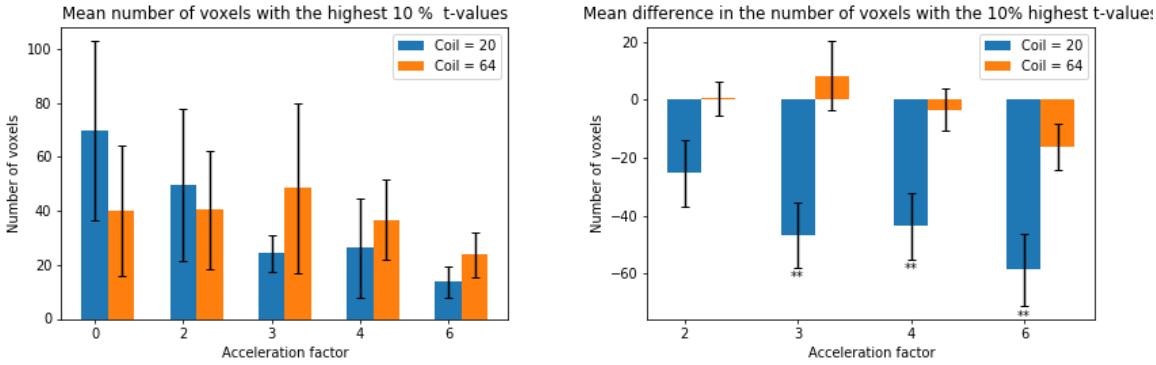

Figure 14: Mean value for the volunters of number of voxels with the 10 % highest t-values (left) and the mean difference between the unaccelerated volume and the accelerated volumes (right) for both the 20 channel and 64 channel head coil. A significance can be seen for acceleration factor 3, 4 and 6 with $p < 0.01$ in the 20 channel head coil.

Significance of the mean difference in number of voxels with the 10% highest t-values between the unaccelerated volume and the accelerated volumes was obtained for acceleration factor 3, 4 and 6 with $p < 0.01$ for the 20 channel head coil. Number of voxels were higher in the unaccelerated volume. The mean value of number of voxels with the 10% highest t-values, mean differences, standard errors and the p-values can be seen in Table 5.

Table 5: Mean number of voxels with the 10 % highest t-values for the volunteers and the mean difference between the accelerated volumes and unaccelerated volume for the volunteers, the standard error of the difference and the p-value calculated from a paired two-tailed t-test. Significant values can be seen in bold

Acc factor	HeadCoil	mean value	mean difference	standard error	p-value
0	64	40.0	-	-	-
2	64	40.5	0.5	5.8	0.933
3	64	48.4	8.4	12.1	0.504
4	64	36.7	-3.3	7.2	0.662
6	64	23.9	-16.1	8.1	0.077
0	20^{+}	69.8	-	-	-
2	20^{+}	44.6	-25.2	11.6	0.058
3	20^{+}	23.2	-46.6	11.2	**0.003**
4	20^{+}	26.2	-43.6	11.6	**0.004**
6	$20^{+\diamond}$	13.9	-55.9	12.5	**0.001**

$^{+}$ Value for subject 6 excluded
$^{\diamond}$ Value for subject 1 excluded

4.2.3 Study with an incomplete paradigm

In the volumes acquired with an incomplete performed paradigm the activation areas were smaller than for the volumes acquired with the correct paradigm, although the difference was

more pronounced for the unaccelerated volume than for the accelerated ones. This can be seen in Figure 15 for one slice for all acceleration factors where both the statistical map with the incomplete paradigm and the correct paradigm can be seen overlaid on a high resolution slice. The slice with the incomplete performed paradigm can be seen in the Figure with blue colour map and the slice with a complete paradigm with red colour map.

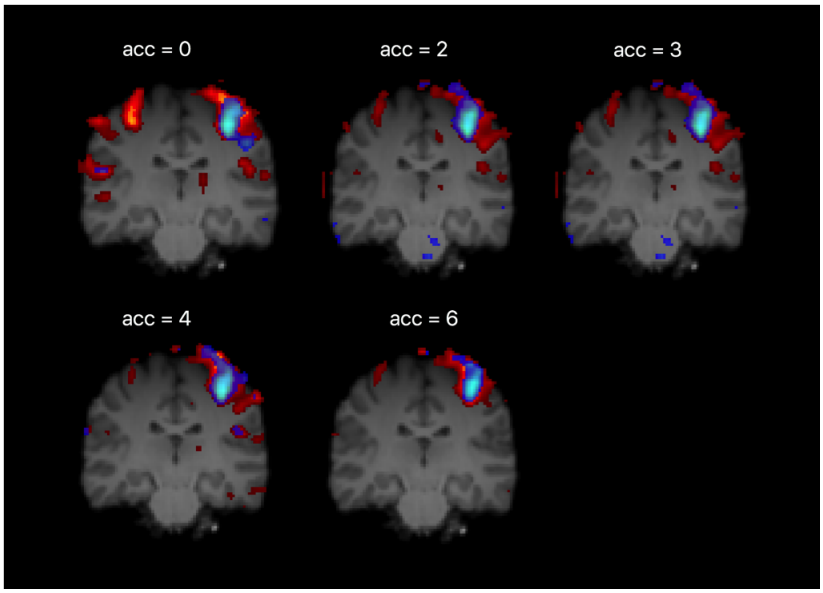

Figure 15: Example images of a slice acquired with the correct paradigm in red and a slice acquired with the incomplete paradigm in blue. The slices are displayed with corresponding high resolution slice.

Number of voxels with t-values over 3.1 decreased with the acceleration factor in contrast to the difference in maximum t-value were highest value was observed for acceleration factor 3 and lowest in the unaccelerated. In Table 6 the relative difference, expressed as percentage between the volume acquired with the correct paradigm and the volume with the incomplete performed paradigm, can be seen.

Table 6: Relative difference in number of voxels with t-values above 3.1 and highest t-value between volumes acquired with the correct performed paradigm and the incomplete paradigm for all acceleration factors.

Acc factor	Relative numb. voxels [%]	Relative max. t-value [%]
0	97%	55%
2	90%	64%
3	87%	64%
4	92%	53%
6	94%	64%

Number of voxels with t-values above 3.1 for the volume acquired with the correct paradigm and the volume acquired with the incomplete paradigm and the difference can be seen in Figure 16 (left). The difference is largest for the unaccelerated volume and decreases with the acceleration factor.

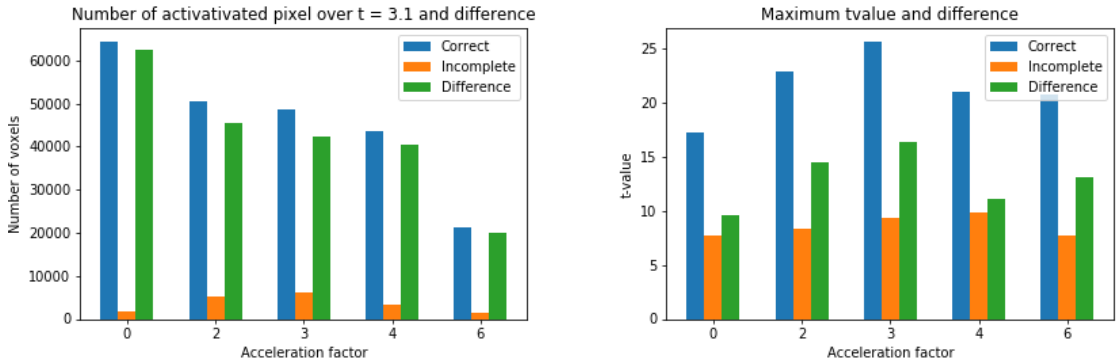

Figure 16: Number of voxels with t-values above 3.1 for the volume acquired with the correct paradigm in blue and for the volume acquired with the incomplete paradigm in orange and the difference in green.

5 DISCUSSION

The aim of this master thesis was to study the multiband EPI pulse sequence and examine how this could be implemented in a clinical setting by finding an optimal acceleration factor to achieve as good temporal resolution as possible without compromising the image quality. Measurements of a water phantom with different coils and acceleration factors were carried out. With help from the phantom measurements result, a protocol for the volunteer measurements was set up. With the volunteer measurements, three different parameters were examined, number of voxels with t-values higher than 3.1 in the segmented volume, number of voxels with the highest 10% of the t-values in the volume and the mean 10 % highest t-value in the volume. With the result from the volunteer measurements, which showed higher t-values for higher acceleration factors in the 64 channel head coil, a study with an incomplete performed paradigm was set up for one volunteer. The aim was to evaluate the difference in t-values between a scan with a paradigm performed as before and a scan with missing blocks in the paradigm. This was an attempt to simulate a patient not able to perform a task correct.

5.1 Phantom measurements

For the water cylinder measurements, a difference in temporal SNR was seen between the 20 channel head coil and the 32 and 64 channel head coil where the 20 channel coil had lower tSNR-values than the other. This due to the fewer coil elements and reflects the inherently superior SNR characteristics of the increasing the number of coil elements. In figure 7 the tSNR seemed to be higher in acceleration factor 2 for the 32 channel head coil compared with the 64 channel. This could be due to the slice selection. There was also a clear decrease in the temporal SNR for the higher acceleration factors but relatively constant for the lowest accelerated volume compared with the unaccelerated ones. The decrease in temporal SNR was both due to higher g-factor noise originating from untangling of superimposed signals and due to a shorter repetition time which gives a decrease in the steady state longitudinal magnetisation. For acceleration factor 2, the reconstruction method is very well conditioned where the simultaneous excited slices are well separated. This leads to a low g-factor noise increase [5] which in turn gives a similar temporal SNR between the accelerated volume and the unaccelerated. Even if the temporal SNR was similar between the 32 channel head coil and the 64 channel head coil for the lower accelerations the decrease in temporal SNR was larger for the 32 channel head coil than for the 64 channel. This is due to generally higher coil sensitivity with a higher number of coil elements. More pronounced artefacts was also seen for the 20 channel coil and the 32 channel coil for the same reason. No difference was seen in temporal SNR and g-factor noise between the two different unaccelerated volumes.

5.2 Volunteer measurements

In order to keep the total experiment duration reasonably short, the examination was performed using only the 20 and 64 channel coils. The standard clinical 20 channel coil was selected as a reference. The 64 channel head coil was chosen due to its superior performance but also since that the coil is slightly less narrow, thus improving potential patient expe-

rience. Because of the pronounced ghosting artefacts and low temporal SNR, acceleration factor 8 was excluded as well. The volunteer results, where the higher acceleration factor exhibited higher t-values suggested that there might be a gain in using higher acceleration factor if the patient has difficulties performing the paradigms.

When examining the motion parameters for all scans, the values were below the limit 1 mm in translation movement and 1 degree for rotational movement. Motion can have a large impact on fMRI analysis but because of the small displacements the uncertainty will in this case be neglected. For subject 1, measurement with acceleration factor 6 failed and had to be discarded for unknown reasons. For subject 8, data acquired with the standard EPI pulse sequence had to be discarded due to unreasonably low activation compared with the accelerated volumes for the same subject.

The temporal SNR decreased with the acceleration factor in the volunteer measurements as well as where the 20 channel head coil had overall lower values. This due to fewer coil elements. A higher temporal SNR was also seen in the outer parts of the brain for both coils, which originates from the higher coil sensitivity. This could also be seen in the EPI-volumes where a lower signal was seen in the center of the brain.

For the 64 channel head coil, the difference in number of voxels with t-values over 3.1 between the unaccelerated volume and the volume acquired with acceleration factor 2 was significant with $p < 0.01$. For acceleration factor 3 and 6, the p-value was close to 0.05. However, number of voxels were higher for the unaccelerated volume for acceleration factor 6. This implies that the number of voxels with t-values above 3.1 increases in moderately accelerated volumes, but decreases with the higher acceleration. As can be seen from the phantom measurements, temporal SNR decreases with the acceleration factor, but the temporal resolution increases as well, where these two will have the opposite effect on the BOLD-sensitivity. This will in turn lead to the non-uniform change in the BOLD-sensitivity as a function of the acceleration factor [5]. No improvement in number of voxels with t-values above 3.1 was seen for the 20 channel head coil.

The difference in the mean 10 % highest t-value in the volume was significant for acceleration factor 2 with $p < 0.05$ for the 20 channel head coil. For the 64 channel head coil the difference was significant for acceleration factor 2 with $p < 0.01$ and acceleration factor 4 with $p < 0.05$. The t-values were higher in the accelerated volumes than the unaccelerated ones, arising from the increasing number of volumes, hence increasing the degrees of freedom on the statistical analysis. However, this also leads to an increase in the temporal autocorrelation which can lead to t-values being overestimated [5]. Although the higher t-values should imply that higher acceleration factors give more credibility in the activation areas. Because only 10 volunteers participated in this study, a more credible result could have been achieved if more volunteers were used.

Previous studies have done similar work where BOLD-sensitivity has been measured for different acceleration factors compared to the unaccelerated. The conclusions drawn were that slice acceleration can be beneficial, but is dependent on anatomical location, where

slice acceleration gives a increase in BOLD-sensitivity in the outer parts of the brain. This is consistent with the result in this study where motor cortex is being measured. Previous studies have come to the conclusion that acceleration factor 2 or higher gives an increase in BOLD-sensitivity which contradicts the result from this study which only saw an increase for acceleration factor 2. [5, 6]. The volunteers had to rest between measurements with the different head coils to reduce influence of weariness in the result. To reduce it even further, a randomisation of acceleration factor order could have been made.

5.2.1 Study with an incomplete paradigm

Because of lack of time only one volunteer was measured for this study. Two volumes each were acquired for the unaccelerated volume and for the volumes with acceleration factors 2, 3, 4 and 6 for the 64 channel head coil. One with a correct performed paradigm, and one with an incomplete performed paradigm. This study was made to simulate a sick patient not able to perform the task completely correct. When studying the volumes with the correct performed paradigm overlaid with the incomplete performed volume, a difference between the acceleration factors was seen, where the unaccelerated volume has lost large activation areas compared with the accelerated volumes. When calculating the difference in number of activated voxels between the two volumes, the smallest difference was seen for acceleration factor 3. This could be due to, although a few blocks in the paradigm is missing, that more data is sampled compared with the unaccelerated volume which gives a higher statistical power. This suggest, although the data is limited, that a higher acceleration can be beneficial if the patient has problem performing the task, but to draw any conclusions more data has to be sampled.

6 CONCLUSION

Results from measurements with the 64 channel head coil provided the following. Number of activated voxels increased for acceleration factor 2 but decreased for higher acceleration factors. Higher t-values were seen in higher acceleration factors but number of voxels with the highest t-values decreased. This meant smaller activation areas with higher t-values were obtained when using accelerated imaging. No advantages were seen with multiband for the 20 channel head coil, but the coil has the advantage of larger size which in a clinical situation sometimes makes it necessary to use. Based on the result, a benefit can be seen in implementing multiband using acceleration factor 2 in a clinical setting for the 64 channel head coil.

In the study with the incompletely performed paradigm, because of the the collective data only consisted of one volunteer, no conclusions can be made. However, this indicates that it can be beneficial to use multiband in a clinical case of a non-compliant patient.

Acknowledgment

I would like to thank my supervisor Peter Mannfolk who have been there helping me and answered questions at all times. Thanks to everyone at the MR-facility, who have helped me with all kinds of problem I have encountered this semester and to all volunteers who have participated.

References

[1] Michael A. Silva, Alfred P. See, Walid I. Essayed, Alexandra J. Golby, and Yanmei Tie. Challenges and techniques for presurgical brain mapping with functional MRI. *NeuroImage: Clinical*, 17:794–803, 2018.

[2] Arne Ekstrom. How and when the fMRI BOLD signal relates to underlying neural activity: The danger in dissociation. *Brain Research Reviews*, 62(2):233–244, mar 2010.

[3] John C. Gore. Principles and practice of functional MRI of the human brain. *Journal of Clinical Investigation*, 112(1):4–9, jul 2003.

[4] Felix A. Breuer, Martin Blaimer, Robin M. Heidemann, Matthias F. Mueller, Mark A. Griswold, and Peter M. Jakob. Controlled aliasing in parallel imaging results in higher acceleration (CAIPIRINHA) for multi-slice imaging. *Magnetic Resonance in Medicine*, 53(3):684–691, 2005.

[5] Nick Todd, Oliver Josephs, Peter Zeidman, Guillaume Flandin, Steen Moeller, and Nikolaus Weiskopf. Functional sensitivity of 2d simultaneous multi-slice echo-planar imaging: Effects of acceleration on g-factor and physiological noise. *Frontiers in Neuroscience*, 11, mar 2017.

[6] Nick Todd, Steen Moeller, Edward J. Auerbach, Essa Yacoub, Guillaume Flandin, and Nikolaus Weiskopf. Evaluation of 2d multiband EPI imaging for high-resolution, whole-brain, task-based fMRI studies at 3t: Sensitivity and slice leakage artifacts. *NeuroImage*, 124:32–42, jan 2016.

[7] Jezzard Matthews Smith. *Functional MRI: An Introduction to Methods*. OXFORD UNIV PR, 2003.

[8] K. Sartor A. L Baert, M. Knauth. *Clinical Functional MRI*. Springer-Verlag GmbH, 2015.

[9] JijaS James, PG Rajesh, Chandrasekharan Kesavadas, and AnuvithaVS Chandran. fMRI paradigm designing and post-processing tools. *Indian Journal of Radiology and Imaging*, 24(1):13, 2014.

[10] Ameera X. Patel and Edward T. Bullmore. A wavelet-based estimator of the degrees of freedom in denoised fMRI time series for probabilistic testing of functional connectivity and brain graphs. *NeuroImage*, 142:14–26, nov 2016.

[11] Julien Dubois and Ralph Adolphs. Building a science of individual differences from fMRI. *Trends in Cognitive Sciences*, 20(6):425–443, jun 2016.

[12] Renat Yakupov, Juan Lei, Michael B. Hoffmann, and Oliver Speck. False fMRI activation after motion correction. *Human Brain Mapping*, 38(9):4497–4510, jun 2017.

[13] L. Muresan, R. Renken, J.B.T.M. Roerdink, and H. Duifhuis. Automated correction of spin-history related motion artefacts in fMRI: Simulated and phantom data. *IEEE Transactions on Biomedical Engineering*, 52(8):1450–1460, aug 2005.

[14] Maxim Zaitsev, Burak Akin, Pierre LeVan, and Benjamin R. Knowles. Prospective motion correction in functional MRI. *NeuroImage*, 154:33–42, jul 2017.

[15] Karl. J. Friston, J. Ashburner, C. D. Frith, J.-B. Poline, J. D. Heather, and R. S. J. Frackowiak. Spatial registration and normalization of images. *Human Brain Mapping*, 3(3):165–189, 1995.

[16] Stephen F. Cauley, Jonathan R. Polimeni, Himanshu Bhat, Lawrence L. Wald, and Kawin Setsompop. Interslice leakage artifact reduction technique for simultaneous multislice acquisitions. *Magnetic Resonance in Medicine*, 72(1):93–102, aug 2013.

[17] Multiband 1: Introduction to sms sequences. https://pdfs.semanticscholar.org/0fce/b0252a10a1a85eb3293dad1836852a5b5eff.pdf. Accessed: 2017-03.

[18] Manushka V. Vaidya, Christopher M. Collins, Daniel K. Sodickson, Ryan Brown, Graham C. Wiggins, and Riccardo Lattanzi. Dependence of b1- and b1 field patterns of surface coils on the electrical properties of the sample and the MR operating frequency. *Concepts in Magnetic Resonance Part B: Magnetic Resonance Engineering*, 46(1):25–40, feb 2016.

[19] Robert J. Anderson, Benedikt A. Poser, and V. Andrew Stenger. Simultaneous multislice spectral-spatial excitations for reduced signal loss susceptibility artifact in BOLD functional MRI. *Magnetic Resonance in Medicine*, 72(5):1342–1352, dec 2013.

[20] Samy Abo Seada, Anthony N. Price, Torben Schneider, Joseph V. Hajnal, and Shaihan J. Malik. Multiband RF pulse design for realistic gradient performance. *Magnetic Resonance in Medicine*, 81(1):362–376, sep 2018.

[21] Markus Barth, Felix Breuer, Peter J. Koopmans, David G. Norris, and Benedikt A. Poser. Simultaneous multislice (SMS) imaging techniques. *Magnetic Resonance in Medicine*, 75(1):63–81, aug 2015.

[22] Mark A. Griswold, Peter M. Jakob, Robin M. Heidemann, Mathias Nittka, Vladimir Jellus, Jianmin Wang, Berthold Kiefer, and Axel Haase. Generalized autocalibrating partially parallel acquisitions (GRAPPA). *Magnetic Resonance in Medicine*, 47(6):1202–1210, jun 2002.

[23] Benedikt A. Poser, Markus Barth, Pål-Erik Goa, Weiran Deng, and V. Andrew Stenger. Single-shot echo-planar imaging with nyquist ghost compensation: Interleaved dual echo with acceleration (IDEA) echo-planar imaging (EPI). *Magnetic Resonance in Medicine*, 69(1):37–47, mar 2012.

[24] Christine Preibisch, J. Gabriel Castrillón G., Martin Bührer, and Valentin Riedl. Evaluation of multiband EPI acquisitions for resting state fMRI. *PLOS ONE*, 10(9):e0136961, sep 2015.

[25] Mark W. Woolrich, Brian D. Ripley, Michael Brady, and Stephen M. Smith. Temporal autocorrelation in univariate linear modeling of FMRI data. *NeuroImage*, 14(6):1370–1386, dec 2001.

[26] Günther Grabner, Andrew L. Janke, Marc M. Budge, David Smith, Jens Pruessner, and D. Louis Collins. Symmetric atlasing and model based segmentation: An application to the hippocampus in older adults. In *Medical Image Computing and Computer-Assisted Intervention – MICCAI 2006*, pages 58–66. Springer Berlin Heidelberg, 2006.

[27] Stefan Geyer, Thorsten Schormann, Hartmut Mohlberg, and Karl Zilles. Areas 3a, 3b, and 1 of human primary somatosensory cortex. *NeuroImage*, 11(6):684–696, jun 2000.

[28] Stefan Geyer, Anders Ledberg, Axel Schleicher, Shigeo Kinomura, Thorsten Schormann, Uli Bürgel, Torkel Klingberg, Jonas Larsson, Karl Zilles, and Per E. Roland. Two different areas within the primary motor cortex of man. *Nature*, 382(6594):805–807, aug 1996.

A APPENDIX

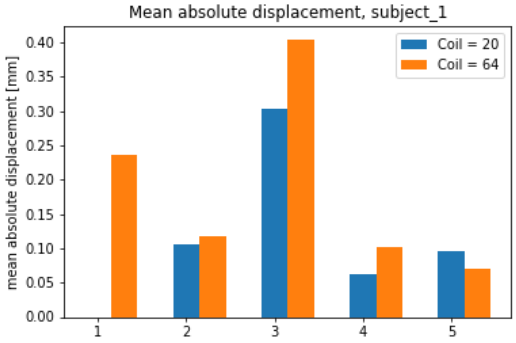
Mean absolute displacement, subject_1
mean absolute displacement [mm]
Coil = 20
Coil = 64
0.00
0.05
0.10
0.15
0.20
0.25
0.30
0.35
0.40
1
2
3
4
5

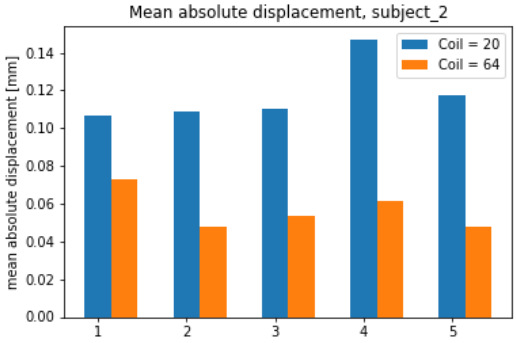
Mean absolute displacement, subject_2
mean absolute displacement [mm]
Coil = 20
Coil = 64
0.00
0.02
0.04
0.06
0.08
0.10
0.12
0.14
1
2
3
4
5

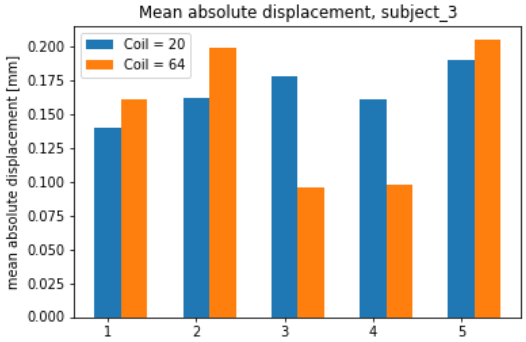
Mean absolute displacement, subject_3
mean absolute displacement [mm]
Coil = 20
Coil = 64
0.000
0.025
0.050
0.075
0.100
0.125
0.150
0.175
0.200
1
2
3
4
5

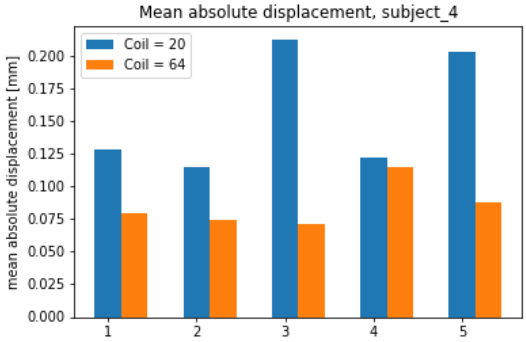
Mean absolute displacement, subject_4
mean absolute displacement [mm]
Coil = 20
Coil = 64
0.000
0.025
0.050
0.075
0.100
0.125
0.150
0.175
0.200
1
2
3
4
5

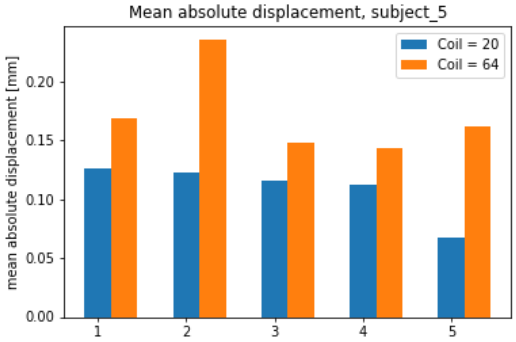
Mean absolute displacement, subject_5
mean absolute displacement [mm]
Coil = 20
Coil = 64
0.00
0.05
0.10
0.15
0.20
1
2
3
4
5

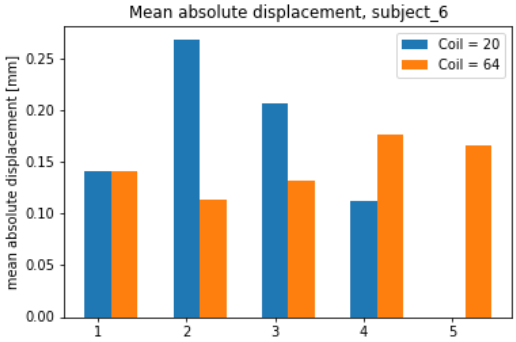
Mean absolute displacement, subject_6
mean absolute displacement [mm]
Coil = 20
Coil = 64
0.00
0.05
0.10
0.15
0.20
0.25
1
2
3
4
5

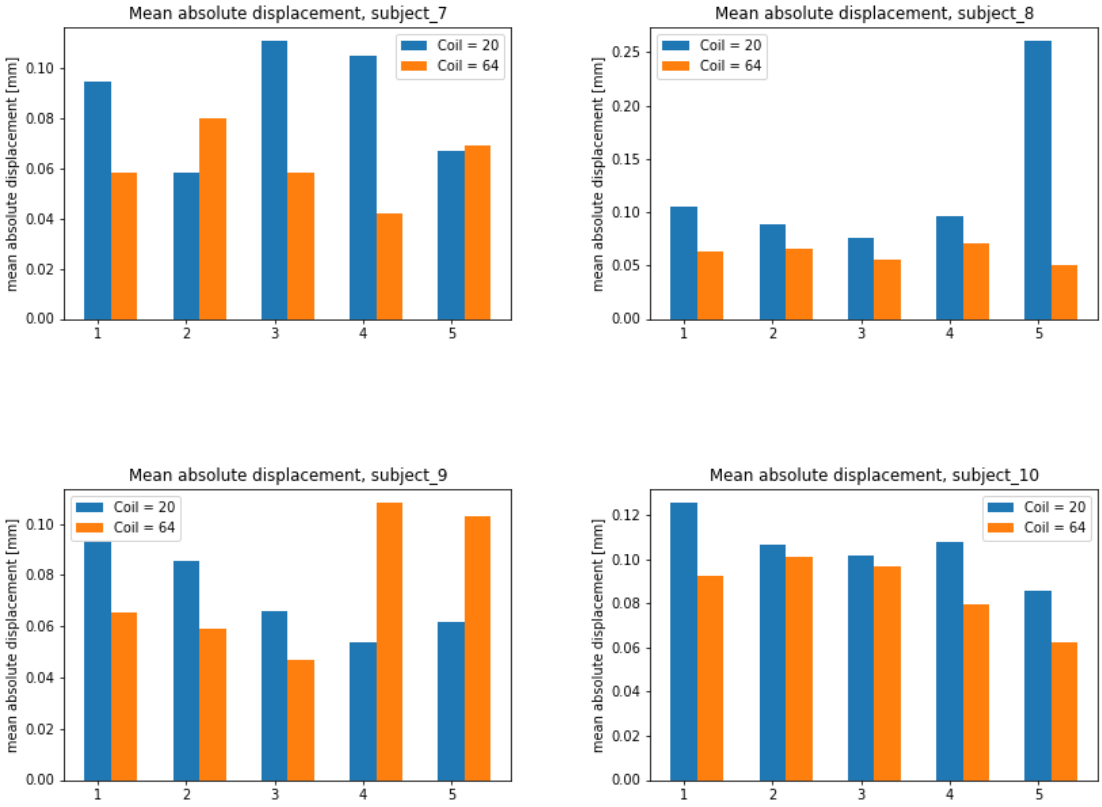

Figure 17: Absolute mean displacement for all volunteers, both for the 64 channel head coil and the 20 channel head coil.

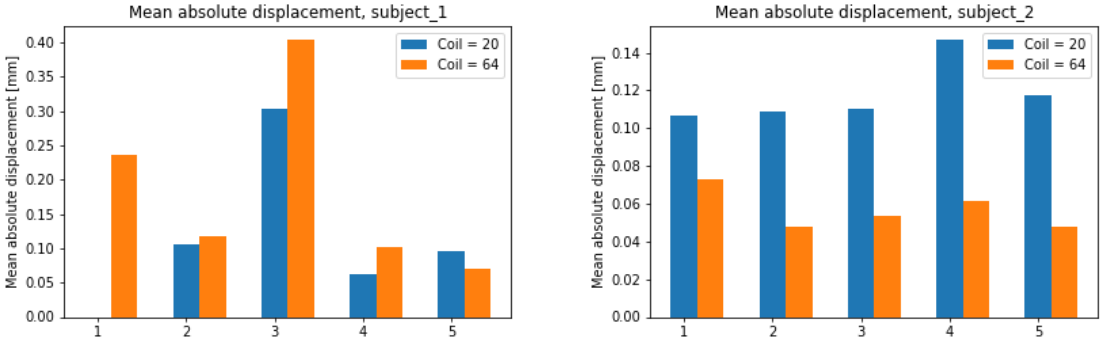

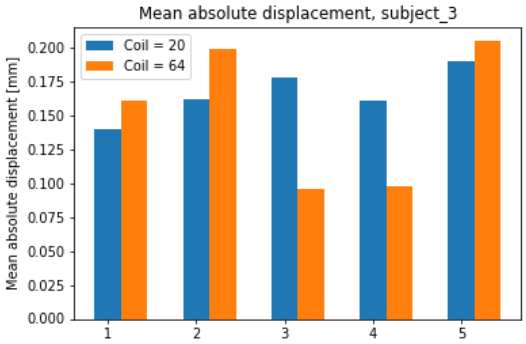
Mean absolute displacement, subject_3
Coil = 20
Coil = 64
Mean absolute displacement [mm]
0.200
0.175
0.150
0.125
0.100
0.075
0.050
0.025
0.000
1
2
3
4
5

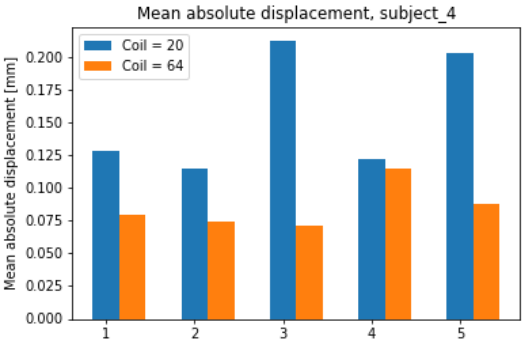
Mean absolute displacement, subject_4
Coil = 20
Coil = 64
Mean absolute displacement [mm]
0.200
0.175
0.150
0.125
0.100
0.075
0.050
0.025
0.000
1
2
3
4
5

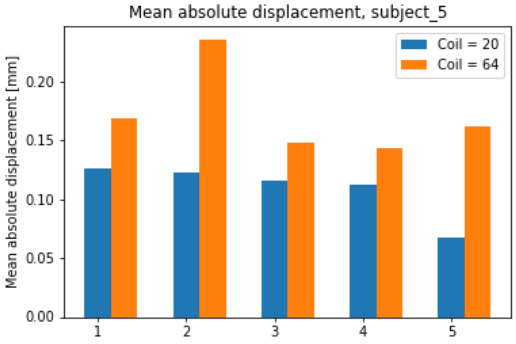
Mean absolute displacement, subject_5
Coil = 20
Coil = 64
Mean absolute displacement [mm]
0.20
0.15
0.10
0.05
0.00
1
2
3
4
5

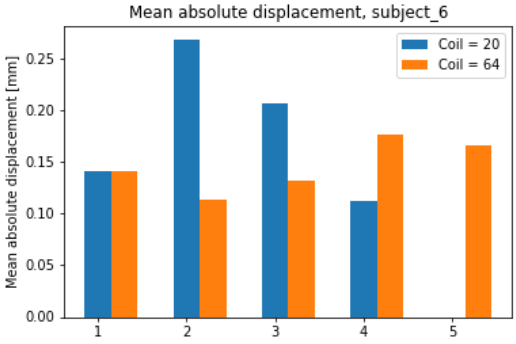
Mean absolute displacement, subject_6
Coil = 20
Coil = 64
Mean absolute displacement [mm]
0.25
0.20
0.15
0.10
0.05
0.00
1
2
3
4
5

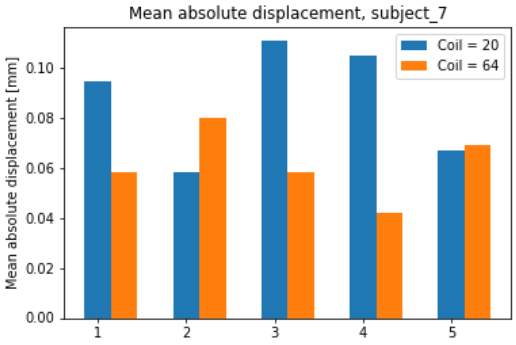
Mean absolute displacement, subject_7
Coil = 20
Coil = 64
Mean absolute displacement [mm]
0.10
0.08
0.06
0.04
0.02
0.00
1
2
3
4
5

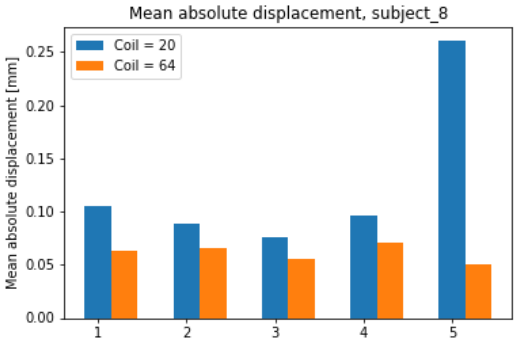
Mean absolute displacement, subject_8
Coil = 20
Coil = 64
Mean absolute displacement [mm]
0.25
0.20
0.15
0.10
0.05
0.00
1
2
3
4
5

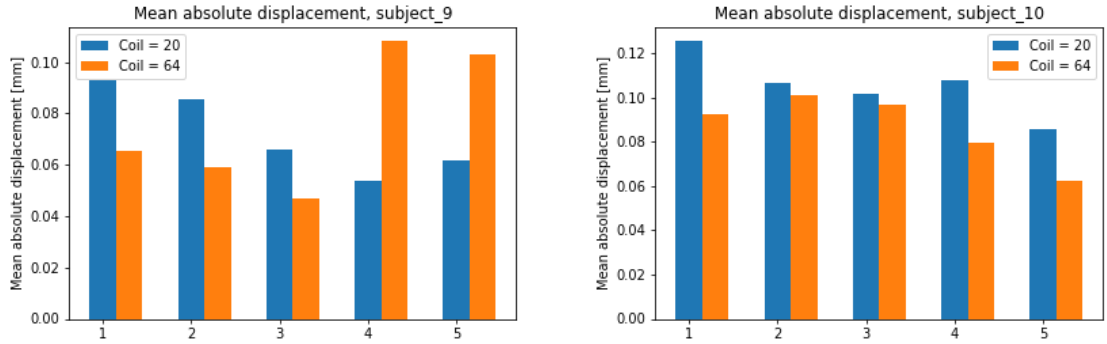

Figure 18: Mean relative displacement for all volunteers, both for the 64 channel head coil and the 20 channel head coil.

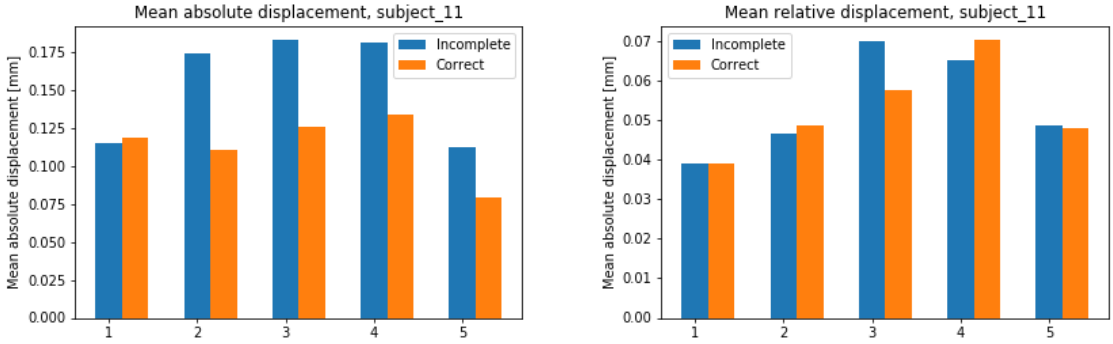

Figure 19: Mean relative displacement and mean absolute displacement for subject 11 performing the correct paradigm and the incomplete paradigm.